High molecular diversity of extraterrestrial organic matter in Murchison meteorite revealed 40 years after its fall

Philippe Schmitt-Kopplin[a,1,2], Zelimir Gabelica[b,1], Régis D. Gougeon[c,1], Agnes Fekete[a], Basem Kanawati[a], Mourad Harir[a], Istvan Gebefuegi[a], Gerhard Eckel[d], and Norbert Hertkorn[a,1]

[a]Helmholtz-Zentrum Muenchen-German Research Center for Environmental Health, Institute for Ecological Chemistry, Ingolstaedter Landstrasse 1, D-85764 Oberschleißheim, Germany [b]Université de Haute Alsace, Ecole Nationale Supérieure de Chimie de Mulhouse, Laboratoire Propre Intégré–Groupe Sécurité et Ecologie Chimiques, 3 Rue Alfred Werner, F-68093 Mulhouse Cedex, France [c]Equipe Eau, Molécules actives, Macromolécules, Activité (EMMA) EA 581, Institut Jules Guyot, Université de Bourgogne, Rue Claude Ladrey, F-21078 Dijon, France [d]Institute of Electronic Music and Acoustics, University of Music and Performing Arts, Inffeldgasse 10/3, A-8010 Graz, Austria

Edited* by Jerrold Meinwald, Cornell University, Ithaca, NY, and approved December 28, 2009 (received for review October 21, 2009).

Numerous descriptions of organic molecules present in the Murchison meteorite have improved our understanding of the early interstellar chemistry that operated at or just before the birth of our solar system. However, all molecular analyses were so far targeted toward selected classes of compounds with a particular emphasis on biologically active components in the context of prebiotic chemistry. Here we demonstrate that a nontargeted ultrahigh-resolution molecular analysis of the solvent-accessible organic fraction of Murchison extracted under mild conditions allows one to extend its indigenous chemical diversity to tens of thousands of different molecular compositions and likely millions of diverse structures. This molecular complexity, which provides hints on heteroatoms chronological assembly, suggests that the extraterrestrial chemodiversity is high compared to terrestrial relevant biological- and biogeochemical-driven chemical space.

Fourier transform ion cyclotron resonance mass spectrometry | interstellar chemistry | nuclear magnetic resonance spectroscopy | organic chondrite | soluble organic matter

Murchison chondrite is one of the most studied meteorites and became a reference for extraterrestrial organic chemistry (1). The diversity of organic compounds recorded in Murchison and in other carbon-rich carbonaceous chondrites (1–5) has clearly improved our understanding of the early interstellar chemistry that operated at or just before the birth of our solar system. More than 70% of the Murchison carbon content has been classified as (macromolecular) insoluble organic matter (IOM) of high aromaticity, whereas the soluble fraction contains extensive suites of organic molecules with more than 500 structures identified so far (6). These structures basically resemble known biomolecules, but are considered to result from abiotic synthesis because of peculiar occurrence patterns, racemic mixtures, and stable isotope contents and distributions. Most of the 100+ kg fragments of Murchison were collected shortly after it fell in Australia on September 28, 1969, so that neither of these fresh samples suffered from intensive terrestrial weathering (7).

As a whole, Murchison is one of the least-altered chondrites (8), recently reclassified by Rubin et al. (9) as CM2.5, where the aqueous alteration index (2.5 petrologic subtype), based on petrographic and mineralogical properties of the meteorite, indicates that the primary lithology of Murchison had experienced a relatively low and uniform degree of aqueous alteration.

Nevertheless, all previous molecular analyses were targeted toward selected classes of compounds with a particular emphasis on amino acids in the context of prebiotic chemistry as potential source of life on earth (10), or on compounds obtained in chemical degradation studies (11) releasing both genuine extractable molecules and reaction products (11–15) often difficult to discern unambiguously.

Alternative nontargeted investigations of complex organic systems are now feasible using advanced analytical methods based on ultrahigh-resolution molecular analysis (16). Electrospray ionization (ESI) Fourier transform ion cyclotron resonance/mass spectrometry (FTICR/MS) in particular, allows the analysis of highly complex mixtures of organic compounds by direct infusion without prior separation, and therefore provides a snapshot of the thousands of molecules that can ionize under selected experimental conditions (17).

Here we show that ultrahigh-resolution FTICR/MS mass spectra complemented with nuclear magnetic resonance spectroscopy (NMR) and ultraperformance liquid chromatography coupled to quadrupole time-of-flight mass spectrometry (UPLC-QTOF/MS) analyses of various polar and apolar solvent extracts of Murchison fragments demonstrate a molecular complexity and diversity, with indications on a chronological succession in the modality by which heteroatoms contributed to the assembly of complex molecules. These results suggest that the extraterrestrial chemical diversity is high compared to terrestrial biological and biogeochemical spaces.

Results and Discussion

FTICR/MS Spectra of Murchison Extracts. A combination of gentle extraction schemes—designed to preserve the authenticity of Murchison organics—consisted in using a few tens of milligrams of uncontaminated material directly removed from the core of three freshly broken distinct Murchison fragments obtained from three different certified sources. These fragments were immediately crushed and extracted in an agate mortar with a few milliliters of various solvents of increasing polarity: toluene and chloroform as apolar aprotic solvents; dimethylsulfoxide (DMSO) and acetonitrile as polar aprotic solvents; and ethanol, methanol, and water as polar protic solvents.

When these extracts were subjected to high field (12 T) FTICR mass spectrometry, several thousands to more than several tens of thousands of highly resolved mass signals were observed within a mass range of 150–1,000 m/z (Fig. 1). The considerable variance of these FTICR mass spectra denotes distinct solvent

Author contributions: P.S.-K. designed research; P.S.-K., Z.G., R.D.G., and N.H. performed research; P.S.-K., A.F., B.K., M.H., I.G., G.E., and N.H. contributed new reagents/analytic tools; P.S.-K., Z.G., R.D.G., A.F., B.K., M.H., I.G., G.E., and N.H. analyzed data; P.S.-K., Z.G., R.D.G., and N.H. wrote the paper; and P.S.-K. and R.D.G. initiated research.

The authors declare no conflict of interest.

*This Direct Submission article had a prearranged editor.

[1]P.S.-K., Z.G., R.D.G., and N.H. contributed equally to this work.

[2]To whom correspondence should be addressed: E-mail: schmitt-kopplin@helmholtz-muenchen.de.

This article contains supporting information online at www.pnas.org/cgi/content/full/0912157107/DCSupplemental.

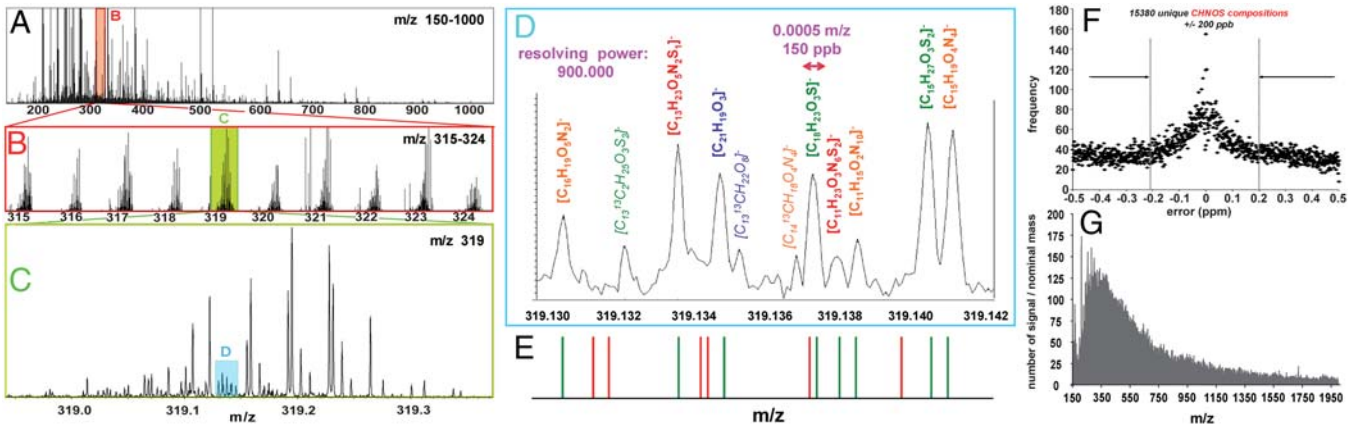

Fig. 1. Progressive detailed visualization of the methanolic Murchison extract in the ESI(–) FTICR/MS spectra in the mass ranges (*A*) 150–1,000 Da, (*B*) 315–324 Da, (*C*) 318.9–319.4 Da, and (*D*) 319.130–319.142 Da with credible elemental formula assignments; (*E*) the bars (red/green) correspond to all 14 possible CHNOS compounds (N, S ≤ 4) in this mass range, which more than half (8 out of 14) were found in the experimental data (green). (*F*) Frequency of assigned elemental formulas as a function of the allowed error windows. (*G*) Distribution of the number of signals per nominal mass [for ESI(+) mode see Fig. S1].

extraction efficiencies with respect to yield as well as to composition (Fig. 2). Error margins routinely as low as <50 ppb in internal calibration (ubiquitous fatty acids) cleared the way to assign individual mass peaks to their corresponding unique elemental compositions within these error levels.

In line with the nominal bulk composition of the Murchinson IOM $C_{100}H_{70}O_{12}N_3S_2$ (18), the attribution of molecular formulas to mass peaks was confined to CHNOS compositions (only a minor suite of phosphorus-containing molecules was identified).

The methanol extract produced the most line-rich mass spectrum in negative-mode electrospray ionization [ESI(−)] FTICR/MS (Figs. 1 and 2): The 150–1,000 Da mass range showed 31,554 singly charged resolved signals at a signal-to-noise ratio (S/N) higher than 2 (113,493 signals at S/N ≥ 1) of which 15,380 could be assigned to CHNOS elemental compositions using an error margin of ±200 ppb (Fig. 1*F*) (29,498 for S/N ≥ 1) leading to 10,299 unique compositions after further filtering (Table 1). In ESI(−) mode, an average number of 125 signals was found in the 350 ± 75 Da nominal mass range with a maximum of up to of 180 resolved signals of singly charged ions within a single nominal mass cluster at an S/N of ≥2 (Fig. 1*F*). The spectrum acquired in the ESI(−) mode delivered 64 $[CHNOS - H]^-$ ionic elemental formulas at the m/z 319 nominal mass ion with up to eleven elemental compositions assigned within only a 10 mDa m/z window (Fig. 1*D*). When considering the neutral nominal mass (CHNOS) at m/z 320 Da, the spectrum acquired in the positive ESI mode [ESI(+)] resulted in 33 distinct $[CHNOS + H]^+$ ionic elemental formulas at the m/z 321 nominal mass ion. Positive and negative ionization modes are complementary (17), and both spectra show repetitive patterns with a high polymolecularity (Fig. 1*A–D* and Fig. S1). When focusing on the m/z 321 mass ion in ESI(+) high-resolution mode, 93 signals could be found within this single nominal mass cluster, all at resolutions exceeding 1.2 million, thus leading to a baseline resolution with m/z differences of only one single mDa (Fig. S1). The compositional diversity revealed in the case of this single methanolic Murchison extract already surpasses that of terrestrial natural organic matter, and even that found in highly chemical diverse petroleum samples (16).

Referring to all extracts, mass peak patterns were consistent with respect to solvent polarities, as shown for the ESI(−) ions at m/z 319 nominal mass (Fig. 2). Except for water, both the polar protic (methanol, ethanol) and aprotic (DMSO, acetonitrile) solvents showed analogous trends in the decrease of the number of molecular compositional series: CHNOS > CHNO > CHOS > CHO (Table 1). Apolar solvents showed a reverse order of molecular composition appearances, namely: CHO > CHNO > CHOS > CHNOS. Because the water extract has been acidified and desalted/concentrated with reverse phase resin solid phase extraction (C18-SPE) prior to mass analysis to avoid the formation of inorganic clusters in the spray, the SPE-based enrichment of Murchison organic matter from the aqueous phase

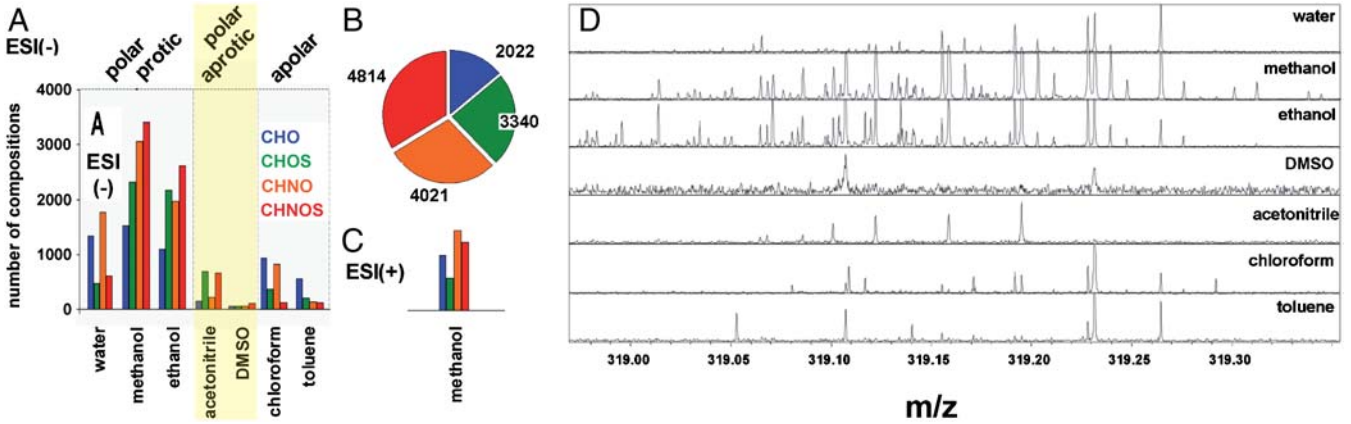

Fig. 2. Extraction efficiency of the solvents. (*A*) Number of total elemental compositions found in ESI(–) mode for the various extraction solvents classified into CHO, CHOS, CHNO, CHNOS molecular series with (*B*) relative distributions of the 14,197 unique compositions attributed to molecular formulas (Table 1). (*C*) Analogous counts and distributions for the ESI(+) mode. (*D*) Section of ESI(–) FTICR/MS spectra between m/z 318.95 and 319.40 Da (nominal mass of neutrals 320 Da) for all solvents, demonstrating the huge chemical diversity of selective extracts.

Table 1. Counts of elemental compositions as a function of extraction solvents and calculation procedures

Ionization mode	Solvent	Number of signals, S/N 2 (S/N 1)	Sum all C, H, O, N (≤3), S (≤3) elemental compositions (200 ppb, N-rule)	Sum all C, H, O, N (≤3), S (≤3) elemental compositions (DBE > 0, H/C < 2.5, O/C < 0)	CHO	CHOS	CHNO	CHNOS
ESI(−)	Water	17,784	6,145	4,170	1,333	470	1,759	608
ESI(−)	Methanol	31,554 (113,493)	15,380 (29,498)	10,299 (12,313)	1,526			
(1,705)	2,311 (2,680)	3,051 (3,473)	3,411 (4,455)					
ESI(+)	Methanol	24,347	8,627	4,540	1,008	598	1,681	1,253
ESI(−)	Ethanol	27,835	11,951	7,852	1,097	2,168	1,969	2,618
ESI(−)	Acetonitril	17,306	3,757	1,720	144	693	217	666
ESI(−)	DMSO	12,741	1,619	264	57	55	48	104
ESI(−)	Chloroform	18,986	4,589	2,236	926	369	815	126
ESI(−)	Toluene	15,532	3,255	994	550	198	129	117
ESI(−)	Total	141,738	46,696	27,535	5,633	6,264	7,988	7,650
ESI(−)	Unique	100,687	26,530	14,197	2,022	3,340	4,021	4,814

depended on hydrophobic interactions and thus consistently showed the order of molecular composition occurrences similar to that observed in the case of apolar solvents (Fig. 2). The methanol extract assigned elemental compositions, and their mass peak intensity produced an average formula of $C_{100}H_{155}O_{20}N_3S_3$ for the extractable organic fraction, showing a higher aliphaticity and oxygen content compared with the Murchison IOM fraction (see above). Previous studies on Murchison IOM already showed that aliphatic structures were most affected by low-temperature chemical oxidations (15).

Indigenous Nature Versus Terrestrial Contamination. The peak abundance in the FTICR mass spectra supports an evaluation strategy whether organics found in Murchison are of indigenous nature (i.e., extraterrestrial) or terrestrial-derived impurities. The mass peaks divide into two categories. First, one could observe several groups of extended, recurring series with an almost continuous intensity distribution across a fairly broad mass range (200–650 Da) contributing over 95% to the peak integral. Second, a few single intense peaks, less regularly distributed across the lower mass range (m/z < 500 Da) were also observed. They almost exclusively belong to CHO and CHOS series rather than to CHNO and CHNOS series (see extracted mass spectra in Fig. S2*A–D*) and likely coincide with fatty and alkyl sulfonic acids by considering exact masses and fragmentation analyses. Components could be systematically annotated to lauric, myristic, palmitic, stearic, icosanoic, and docosanoic acids in the C_{12} to C_{22} series of $C_xH_yO_2$ molecules. In addition, the most intense mass peaks of the second category correspond mainly to dioxygenated molecules and exhibit a more distinctive preference of even number of carbon over odd number than those corresponding to other extended recurring molecular series. The suggested contaminant contributions probably arise from terrestrial bio(geo)chemistry not necessarily exclusive but likely additive to indigenous Murchison organic matter [the even-to-odd ratio was, on average, 1.70 for the 35 most intense signals of $C_xH_yO_2$ calculated formulas and close to one (0.99) for the 233 other less intense signals].

The Murchison solvent soluble bulk composition with a H/C ratio near unity (see van Krevelen diagrams in Fig. S2*E–J*) implies that even regarding its (primarily) nonterrestrial provenance, the methylene (-CH_2-) group will remain the most relevant nominal building block of its organic chemistry, and a (-CH_2-)-based Kendrick mass defect (KMD) analysis (16, 17) is very instructive in revealing its compositional diversity (Fig. S3*A–E*). The peak richness of the observed patterns gives evidence of the intrinsic compositional (and structural) diversity of molecules within and across chemical classes, which is an acknowledged feature of extraterrestrial chemistry (19, 20). Comparable but lesser diversity was also found in terrestrial organic matter (17) as well as in chemically complex products of reactions modeling processes that possibly take place in Titan's atmosphere (21). The occurrence of extensive homologous (-CH_2-)-series is an inevitable consequence of intricacy within organic mixtures (17), so analogous regular patterns do appear in the various data reduced to two-dimensional depictions of mass spectra (e.g., van Krevelen diagrams), which reflect projections of the CHNOS compositional space (Fig. 3 and Figs. S1, S2, and S3). The CHO series showed the lowest initial and average KMD values followed by the CHNO compounds. The presence of sulfur caused systematic KMD displacements to higher values for CHOS and CHNOS, respectively (Fig. S3*A–D*).

The regularity of mass peak patterns (Fig. S2*A–D*) also reflects itself in the conformity of mass peak intensity distributions for CHO, CHNO, CHOS, and CHNOS compositions within each series for single nominal masses (example given in Figs. 1 and 2 and Fig. S1*E–H* for negative ion masses 319 and 431 Da) as well as across the entire mass range.

The structural diversity of the Murchison extracts is also reflected by a considerable variability of their NMR spectra and refers to a wide range of aliphatic and aromatic chemical environments with substantial contributions from heteroatoms (Fig. S4*A–N*). The reverse phase gradient UPLC-QTOF/MS analysis of the methanol and acetonitrile extracts led to the separation of a total of 683 compounds (only 223 common to both solvents) with many successions of extended homologous series (e.g., separated by m/z 44 and m/z 14) as observed in the chromatograms/mass spectra (Fig. S5). These series reflect analogous compositional sequences as observed in the van Krevelen elemental ratio and KMD visualizations of FTICR/MS data. In order to confirm these trends, we have performed a functional group analysis by computing the number of peak doublets separated by specific m/z differences attributed to the major functional groups at 0.5 ppm confidence limit (Fig. S3*F*). For example, an assessment of all CH_2-doublets would identify all adjacent mass peaks within given classes of KMD in all rows of a CH_2-Kendrick diagram (Fig. S3*E*). Interestingly, the (-CH_2-) (mass defect 14.016 Da), (-COOH) (mass defect 43.990 Da) and (-OH) (mass defect 15.995 Da) functional groups show the same graduation of frequencies between the CHO, CHOS, CHNO, and CHNOS series. Nitrogen-containing fragments were only identified in CHNO and CHNOS series, whereas sulfur-containing components were naturally found in CHOS and CHNOS series in the form of (-SO_3) (mass defect 79.957 Da) and twice more frequently in the form of (-SH) (mass defect 31.972 Da; Fig. S3*F*), thereby corroborating the utility of mass differences in the functional group analysis of complex materials. Nitrogen occurred basically as (-NH-) (mass defect 15.011 Da) and less as (-NH_2) (mass defect 16.019 Da) or single (-N-) (mass defect 14.003 Da). Therefore, in the mass range explored, most of the nitrogen would be found as amide or heterocyclic moieties, whereas amine and amino acid classes are expected to be much less prevalent. This deviation from

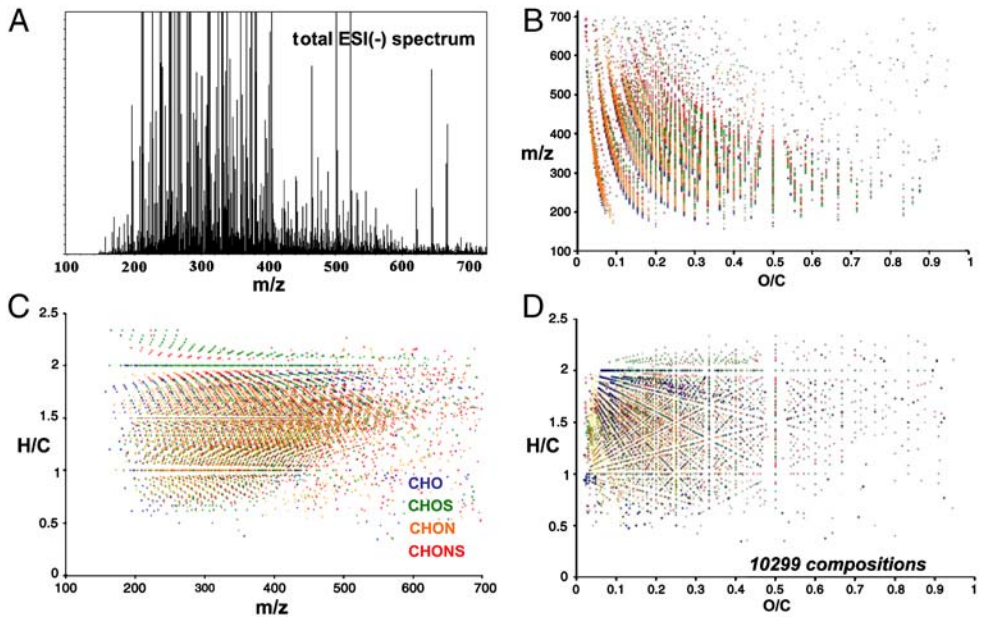

Fig. 3. Integrated representations of the molecular diversity in the methanol extracted fraction, derived from ESI(–) FTICR/MS spectra in the (*A*) 150–700 *m*/*z* range. (*B–D*) Relationships between *m*/*z*, H/C, and O/C elemental ratios corresponding to the mass spectra shown in *A*.

acknowledged values for Murchison (1) is readily explained considering that almost all of the previously identified N-containing molecules exhibit masses lower than 150 Da, a mass range not covered in our FTICR/MS analysis.

Sulfur Chemistry Chronology. The four series of molecules (CHO, CHOS, CHNO, and CHNOS) showed two very distinct distributions of mass peaks (Figs. 3 and 4 and Fig. S2*A–D*): CHO and CHOS series exhibited an almost continuous increase of their mass peak intensities following an ascending H/C ratio (H-rich aliphatic compounds). In contrast, CHNO and CHNOS series exhibit a slightly skewed near Gaussian distribution of their mass peak intensities with large occurrences of mass peaks at average H/C ratios (Fig. 4). These trends are observed over the entire mass range recorded on the spectra (Fig. S6*A–D*). Such a procedure to visualize data also allows one to rapidly spot the presence of peaks caused by impurities. These distinct mass profiles imply a strong directional relationship between the CHO and CHOS series on the one hand and the CHO and CHOS series on the other hand and therefore suggest separate histories of formation and evolution for CHNO and CHNOS compounds and for their S-bearing analogues. The mass peak intensity distribution depicted as a function of the number of oxygen atoms in CHO versus CHOS and CHNO versus CHNOS series indicated that an increase in S was followed by an increase in oxygen all over the mass range, suggesting the occurrence of sulfur in elevated oxidation states (Figs S6*E–H*, S7, and S8*A–D*).

Links Toward the Origin of Murchison Organic Matter. Many of the small molecules originally identified in protoplanetary disks (e.g., CO, CN, CS, H_3COH) are expected to be reactive under conditions of nebulae evolution (18). Already, the rather abundant formaldehyde ($H_2C=O$) and HCN molecules alone produce an opulent and well-investigated intra- and intermolecular chemistry with an amazing diversity of intricate reaction products, leading to CHO, CHN, and CHNO series of molecules, respectively. In addition, in reducing atmosphere of CH_4, NH_3, and CO at low temperatures (e.g. 10–20 K) and strong irradiation regimes, conditions that initially characterized the early primordial nebula chemistry, aromatic nitrogen heterocycles, and other similarly hydrogen-deficient molecules are readily formed. It seems that extrusion of hydrogen from organic intermediates is one of the main reactions enabling this outcome. These molecules are relatively silent at low temperatures, although long-term irradiation will likely induce radical formation and recombination with subsequent loss of precursor signature. However, hydrothermal processing might impose drastic alterations, one of which is processing toward a CHO series of molecules that are more soluble than CHNO molecules and therefore will show divergent mass peak signatures.

During its trajectory of formation, the Murchison meteorite has sampled across a huge variety of spatial, compositional, temperature, and irradiation regimes as evidenced from, e.g., the variance in composition of tiny enclosed mineral grains (9). Although less cleary discernible from complex mixtures when

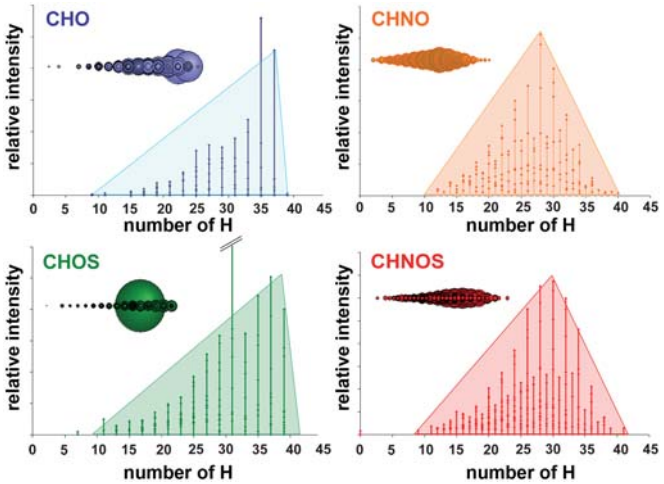

Fig. 4. Distribution of mass peaks within the CHO, CHOS, CHNO, and CHNOS series for molecules with 19 carbon atoms. CHO and CHOS series exhibit increasing intensities of mass peaks for aliphatic (hydrogen-rich) compounds, whereas CHNO and CHNOS series exhibit a slightly skewed near Gaussian distribution of mass peaks with large occurrences of mass peaks at average H/C ratio. The apparent odd/even pattern in the CHNO and CHNOS series denotes occurrence of even (N_2) and odd ($N_{1,3}$) counts of nitrogen atoms in CHNO(S) molecules in accordance with the nitrogen rule (Fig. S8*E*).

using low-resolution structural and compositional analysis, organic chemistry features vastly enhanced opportunities of forming different chemical structures in comparison with minerals. Constraints of temperature, radiation, accessibility, and selectivity of reaction pathways (e.g., aromatization) have likely guided the trajectory of organics evolution into a complex mixture, eventually approaching an entropy-driven near continuous distribution of molecular compositions and structures characteristic of abiotic syntheses, with a loss of distinct precursors signature. Those thermodynamic and kinetic constraints under conditions of meteorite evolution might fundamentally deviate from terrestrial biogeochemistry under oxygen atmosphere and ambient temperature. Furthermore, episodal or long-term events and regime chances like strong irradiation (from sun or some nearby supernovae) or parent body hydrothermal processing might have altered the bearing of the general trajectory of reactivity, not necessarily with uniform effects across the entire parent body. Therefore, spatial (physical and chemical) heterogeneity on nano-, micro-, and macroscales might then be the rule rather than the exception for nonprocessed meteorites and their parent bodies.

The presolar organic synthesis appears feasible already in the lower 10 K range in the outer space (2, 22) and at higher temperatures; for instance, the UV photolysis of atmospheric aerosols is the key to typical CHN(O) organic chemistry at around 90 K observed on Titan (21, 23).

Bulk aqueous hydrolysis of organic matter is unlikely to occur in the cold space in contrast to oxygenation initiated by radical recombination. Elevated temperatures required for hydrothermal organic alterations can be caused by impacts, radiogenic heating (^{26}Al, ^{60}Fe) during the dawn of the solar system, proximity to the sun, or parent body processing. Aqueous alteration in CM-type chondrites occurred mainly on their respective parent bodies (5, 9, 24) as deduced from petrography and element/isotopic ratios (9), although organic complexity itself so far has precluded a meaningful assessment of its heritage. In general, organics are more susceptible to thermal alteration than most minerals such as silicates, oxides, and other presolar grains found in meteorites. It is considered, though, that in several carbonaceous chondrites, the organic chemistry is intimately linked to the fate of the inorganic bulk that hosts it (25, 26).

Catalytic liquid-solid reactions on the parent body, particularly aqueous alteration (27, 28), are believed to have supported the formation of various suites of amino and carboxylic acids through Strecker-like reactions (29–31) in line with the significant extent of oxygen functionalization observed in the Murchison organic matter. Aqueous alteration is related to the occurrence and relative abundance of silicate minerals (8, 30). Clay-like (alumino) silicates and phyllosilicates in particular are considered to promote organic matter accumulation in extraterrestrial environments (9, 32) and could have acted as catalysts for the formation of polar compounds (2, 33), hosts for acidic or basic N-heterocycles (chemisorption lead to selective protection), and possibly also for the polymerization of light hydrocarbons as shown recently for terrestrial sediments (34).

Aqueous alteration and terrestrial weathering/contamination might be discriminated based on, e.g,. odd/even preferences within molecular series (reflecting biogenic heritage), whereas heating and ablation during the atmospheric entry would show a characteristic compositional anisotropy from the rim to the core, thus amenable to depth-profiling.

The observed peak intensity distribution of CHNO (and CHNOS) series follows the feasible count of chemically relevant isomers; i.e., at intermediate H/C ratios, the possibilities of forming different isomers are at maximum (17). Hence, the observed peak patterns reflect the expected distribution at (near) maximum entropy in which any mass peak represents a superposition of isomers defined by a proportionate relationship between mass peak intensities and feasible numbers of chemically relevant isomers. The apparent odd/even pattern for CHNO and CHNOS series in Fig. 4 reflects the decreasing occurrence of nitrogen-containing molecules ($N_1 > N_2 > N_3$) in the CHNO and CHNOS series; an analogous decrease ($S_1 > S_2 > S_3$) is observed for sulfur-containing molecules (Fig. S8*E–I*).

The sizable hydrogen deficiency of CHNO molecules suggests a significant occurrence of heterocyclic nitrogen in Murchison organic matter anticipated already from differential mass spectra (compare above). Continual incorporation of (hydrogen-deficient) HCN during the formation of CHNO molecules would have contributed to confine the average H/C ratio of products to the intermediate or even low levels, as observed.

The observed variation of mass peak distributions (Fig. 4 and Fig. S6*A–D*) indicated a chronological sequence of the Murchison organic matter evolution, possibly initiated by the formation of a complex core of CHNO molecules.

The mass peak intensities of CHO molecules generally increased with the H/C ratio, indicating prominence of aliphatic structures. A fraction of singular peaks with especially large mass peak intensities likely includes contributions from terrestrial contamination, nevertheless in addition to (major) pristine meteorite organic matter.

Hence, the fundamental variance in the distribution of CHO and CHNO molecules and their average H/C ratios would either imply divergent formation pools and timelines or differential processings of source materials into soluble hydrogen-rich (aliphatic) CHO molecules, e.g., by hydrothermal events and/or preferential oxidation of aliphatic over (extended) aromatic structures.

The in essence unaltered mass peak distribution in the presence and absence of sulfur is remarkable and could imply subsequent addition of sulfur functionalities onto CHNO (and CHO) precursor molecules. A reverse order in which desulfurization (from CHNOS into CHNO or from CHOS into CHO series) would have left the respective mass peak distributions unaltered appears less conceivable because of entropy considerations. Alternatively, a neutral collective chemical impact of sulfur incorporation on the relative unsaturation (H/C ratio) appears feasible. Like oxygen, sulfur can formally be inserted into any C-C and C-H bond; however additional variance exists because of accessible formal sulfur oxidation states in the range of −2 to +6. Variance in sulfur oxidation would rather affect the O/C ratios compared to H/C ratios. Indeed, it is shown here that the increase in sulfur parallels with the increase in oxygen (Fig. S6*E–H*), indicating the occurrence of oxygenated sulfur groups in Murchison extracts.

As an example of sulfurization, under the hypothesis of a single formal insertion of OSO_2 into C-H bonds of CHO and CHNO compounds to address the occurrence of oxidized sulfur in Murchison, more than 30% of the obtained theoretical elemental compositions were found in the experimentally discovered CHOS and CHNOS series, respectively (Fig. S2*I–J*). An abiotic sulfurization of the organic matter has been observed at low-temperature and neutral pH (5, 35). Whereas thiophenes dominate the speciation of sulfur in terrestrial petroleum, processed bitumen contains oxidized organic sulfur species such as sulfoxides, sulfones, sulfonates, and sulfates (36). The contribution of inorganic sulfur chemistry not yet considered here might be important or even pivotal to the Murchison organic chemical diversity. The Murchison meteorite contains various iron sulfides such as FeS (troilite), paramagnetic FeS_2, Fe_3S_4 (greigite) (37), a few nonstoichiometric $FeS_{1-x}S$ pyrrhotite polytypes (38), or mixed Fe-Ni sulfides such as pentlandite $(Fe,Ni)_9S_8$ (39). Such minerals, although known to be rather nonreactive in frozen meteorites, might react with CHO and CHNO molecules in various ways (i.e., catalysis) in the presence of warm water or through certain solid-state reactions under mild temperature conditions. Accordingly, reactions of such Fe_xS_y phases with preassembled CHO and

CHNO molecules through, e.g., initial S insertion might present an alternative pathway for synthesis of the respective CHOS and CHNOS series.

So far, the mass spectrometry analysis of Murchison organic matter has been focused upon ESI(−) FTICR mass spectra of methanol extracts. In extension, a total of 46,696 elemental compositions corresponding to 14,197 distinct elemental formulas were found in the consolidated ESI(−) FTICR mass spectra of all extracts combined together (out of a total of >150,000 mass peaks under conservative calculations). Previous studies on natural organic matter (17) showed that ESI(−) FTICR mass spectra represented only about one-third of the total consolidated number of mass peaks and assigned elemental formulas when complementary ionization techniques were used in combination (atmospheric pressure photoionization, chemical ionization, and ESI in positive and negative modi). A proportional scaling in the case of Murchison organic matter would project into an excess of 50,000 elemental formulas. In addition to the large number of signals, the pronounced regularity of signal patterns is typical of entropy-driven synthesis while leading to a high diversity of isomeric compounds (an audio-translation/sonification of some selected mass spectrometric data can be compared by listening to the corresponding files as described in Fig. S9). The isomeric diversity of these extraterrestrial organics (40), with the given respectable size and heteroatom content of assigned compositions (17), would then lead to a realistic minimum of several thousands of isomers for any given elemental composition in Murchison organic matter. Then, several millions of different chemical compounds might be present in carbonaceous chondrites as a result of abiotic chemistry, implying the six major elements involved in life, namely, C, H, O, N, S (and P).

The combination of high-resolution structure-selective analytical methods involved here, composed of organic structural spectroscopy in the form of FTICR/MS, UPLC-QTOF-MS, and NMR, will more readily lead to an educated handling of organic and inorganic meteorite molecular complexity when supplemented with spacial resolving techniques such as nano–secondary ion mass spectrometry, extended x-ray absorption fine structure spectroscopy, and x-ray-microscopy,. This will eventually elevate the scientific appreciation of interstellar molecules formation and, e.g., organomineral interactions shaping the respective selectivity to a high level of comprehension, with benefits to the scientific assessment of extraterrestrial chemistry in general and planetary disk evolution in particular.

Materials and Methods

Samples. Three different Murchison samples were used for all measurements. They were obtained from three different sources, namely from Eric Twelker (Juneau, Alaska; code ET 06674), Dirk Ross (Tokyo; code DR 07625), and Guy Heinen (Linger, Luxembourg; code GH 08729). The use of three different samples and variable handling of each fragment allowed us to confirm the possible discrimination between genuine organic contents in Murchison and possible terrestrial contaminations in the mass spectra.

Procedures describing sample preparation, FTICR/MS analyses, and other experimental details are given in *SI Text*.

1. Sephton MA (2002) Organic compounds in carbonaceous meteorites. *Nat Prod Rep* 19:292–311.
2. Remusat L, Derenne S, Robert F, Knicker H (2005) New pyrolytic and spectroscopic data on Orgueil and Murchison insoluble organic matter: A different origin than soluble. *Geochim Cosmochim Acta* 69:3919–3932.
3. Alexander CMO, Fogel M, Yabuta H, Cody GD (2007) The origin and evolution of chondrites recorded in the elemental and isotopic compositions of their macromolecular organic matter. *Geochim Cosmochim Acta* 71:4380–4403.
4. Pizzarello S, Cooper GW, Flynn GJ (2006) *Meteorites and the Early Solar System II* (Univ. of Arizona Press, Tucson, AZ), pp 625–651.
5. Busemann H, et al. (2006) Interstellar chemistry recorded in organic matter from primitive meteorites. *Science* 312:727–730.
6. Cronin JR (1998) *The Molecular Origins of Life: Assembling Pieces of the Puzzle*, ed Brack A (Cambridge Univ. Press, Cambridge, UK), pp 119–146.
7. Zolensky ME, Gooding JL (1986) Aqueous alteration on carbonaceous-chondrite parent bodies as inferred from weathering of meteorites in Antarctica. *Meteoritics* 21:548–549.
8. Browning LB, McSween HY, Zolensky ME (1996) Correlated alteration effects in CM carbonaceous chondrites. *Geochim Cosmochim Acta* 60:2621–2633.
9. Rubin AE, Trigo-Rodriguez JM, Huber H, Wasson JT (2007) Progressive aqueous alteration of CM carbonaceous chondrites. *Geochim Cosmochim Acta* 71:2361–2382.
10. Chyba CF, Sagan C (1992) Endogenous production, exogenous delivery and impact-shock synthesis of organic molecules: An inventory for the origins of life. *Nature* 355:125–132.
11. Hayatsu R, Matsuoka S, Scott RG, Studier MH, Anders E (1977) Origin of organic matter in the early solar system. VII. The organic polymer in carbonaceous chondrites. *Geochim Cosmochim Acta* 41:1325–1339.
12. Khomiya M, Shimoyana A (1996) Organic compounds from insoluble organic matter isolated from the Murchison carbonaceous chondrite by heating experiments. *Bull Chem Soc Jpn* 69:53–58.
13. Cronin JR, Pizzarello S (1987) ^{13}C NMR spectroscopy of insoluble carbon of carbonaceous chondrites. *Geochim Cosmochim Acta* 51:299–303.
14. Gardiner A, et al. (2000) Solid state ^{13}C NMR of the insoluble organic matter of the Orgueil and Murchison meteorites: Quantitative study. *Earth Planet Sci Lett* 184:9–21.
15. Cody GD, Alexander CMO (2005) NMR studies of chemical structural variation of insoluble organic matter from different carbonaceous chondrite groups. *Geochim Cosmochim Acta* 69:1085–1097.
16. Marshall AG, Rodgers RP (2008) Petroleomics: Chemistry of the underworld. *Proc Natl Acad Sci USA* 105:18090–18095.
17. Hertkorn N, et al. (2008) Natural organic matter and the event horizon of mass spectrometry. *Anal Chem* 80:8908–8919.
18. (2006) *Meteorites and the Early Solar System II*, ed Dante S (The University of Arizona Space Sciences Series), General ed p 943.
19. Davis AM (2005) Treatise on Geochemistry. *Meteorites, Comets and Planets*, ed Holland HD (Elsevier) p 736.
20. Cronin JR, Pizzarello S, Epstein S, Krishnamurthy RV (1993) Molecular and isotopic analyses of the hydroxy acids, dicarboxylic acids, and hydroxydicarboxylic acids of the Murchison meteorite. *Geochim Cosmochim Acta* 57:4745–4752.
21. Somogyi A, Oh C-H, Smith MA, Lunine JI (2005) Organic Environments on Saturn's Moon Titan: Simulating Chemical Reactions and Analyzing Products by FT-ICR and Ion-Trap Mass Spectrometry. *J Am Soc Mass Spectr* 16:850–859.
22. Endress M, Zinner E, Bischoff A (1996) Early aqueous activity on primitive meteorite parent bodies. *Nature* 379:701–703.
23. Boss AP (2002) Astrobiological implications of forming the solar system in an ultraviolet-rich environment. *Astrobiology* 4:523–524.
24. Summons RE, Albrecht P, McDonald G, Moldowan JM (2008) Molecular biosignatures. *Space Sci Rev* 135:133–159.
25. Pearson VK, et al. (2002) Clay mineral-organic matter relationships in the early solar system. *Meteorit Planet Sci* 37:1829–1833.
26. Schulte M, Shock E (2004) Coupled organic synthesis and mineral alteration on meteorite parent bodies. *Meteorit Planet Sci* 39:1577–1590.
27. Macdougall JD, Lugmair GW, Kerridge JF (1984) Early aqueous activity on primitive meteorite parent bodies. *Nature* 307:249–251.
28. Zolensky M, McSween HY (1988) *Meteorites and the Early Solar System*, ed Kerridge JF (University of Arizona Press, Tucson, AZ), pp 114–143.
29. Lerner NR, Cooper GW (2005) Iminodicarboxylic acids in the Murchison meteorite: Evidence of Strecker reactions. *Geochim Cosmochim Acta* 69:2901–2906.
30. Pizzarello S, Zolensky M, Turk KA (2003) Nonracemic isovaline in the Murchison meteorite: Chiral distribution and mineral association. *Geochim Cosmochim Acta* 67:1589–1595.
31. Glavin DP, Dworkin JP (2009) Enrichment of the amino acid L-isovaline by aqueous alteration on CI and CM meteorite parent bodies. *Proc Natl Acad Sci USA* 106:5487–5492.
32. Pearson VK, Kearsley AT, Sephton MA, Gilmour I (2007) The labelling of meteoritic organic material using osmium tetroxide vapour impregnation. *Planet Space Sci* 55:1310–1318.
33. Hartman H, Sweeney MA, Kropp MA, Lewis JS (1993) Carbonaceous Chondrites and the Origin of Life. *Origins Life Evol Biosphere* 23:221–227.
34. Antia DDJ (2008) Oil polymerisation and fluid expulsion from low temperature, low maturity, over-pressured sediments. *J Petrol Geol* 31:263–282.
35. Schaeffer P, Reiss C, Albrecht P (1995) Geochemical study of macromolecular organic matter from sulfur-rich sediments of evaporitic origin (Messinian of Sicily) by chemical degradations. *Org Geochem* 23:567–581.
36. Brown JR, Kasrai M, Bancroft GM, Tan KH, Ghen J-M (1992) Direct identification of organic sulphur species in Rasa coal from sulphur L-edge x-ray absorption near-edge spectra. *Fuel* 71:649–653.
37. Levin EM, Bud'ko SL, Mao JD, Huang Y, Schmidt-Rohr K (2007) Effect of magnetic particles on NMR spectra of Murchison meteorite organic matter and a polymer-based model system. *Solid State Nucl Magn Reson* 31:63–71.
38. Zolensky ME, Thomas KL (1995) Iron and iron-nickel sulfides in chondritic interplanetary dust particles. *Geochim Cosmochim Acta* 59:4707–4712.
39. Binet L, Gourier D, Derenne S, Robert F (2002) Heterogeneous distribution of paramagnetic radicals in insoluble organic matter from the Orgueil and Murchison meteorites. *Geochim Cosmochim Acta* 66:4177–4186.
40. Kvenvolden K, et al. (1970) Evidence of extraterrestrial amino acids and hydrocarbons in the Murchison meteorite. *Nature* 228:923–926.

Supporting Information

Schmitt-Kopplin et al. 10.1073/pnas.0912157107

SI Text

SI Material and Methods. ***Fourier Transform Ion Cyclotron Resonance/Mass Spectrometry Analysis.*** A few freshly broken fragments of a total weight of about 30 mg removed from the core of each sample were first washed by stirring for a few seconds within the extraction solvent prior to crushing with an agate pillar in 1 mL solvent poured into the corresponding agate mortar. This procedure was shown to limit the number of signals resulting from terrestrial and human contamination, for example, fatty acids arising from sample handling. The mixture (suspension) was transferred into a vial and submitted to an ultrasonic cleaning for not more than 10 min, then centrifuged. The supernatant liquid was readily removed with a microsyringe, ready for flow injection into the ESI-source.

Samples were introduced into the microelectrospray source at a flow rate of 120 μL/h with a nebulizer gas pressure of 20 psi (138 kPa) and a drying gas pressure of 15 psi (103 kPa) at 200 °C (Agilent sprayer). Spectra were first externally calibrated on clusters of arginine (1 mg/L in methanol), and internal calibration was systematically performed with fatty acids present reaching accuracy values lower than 0.05 ppm in routine day-to-day measurements. The spectra were acquired with a time domain of 4 megawords in the mass range of 100–2,000 m/z for a peak resolution >500,000 at m/z 400, reaching 1 million at m/z 250. Up to 5,000 scans were accumulated for each sample.

Fourier transform ion cyclotron resonance (FTICR) spectra with m/z from 150 to 2,000 were exported to peak lists at a signal-to-noise ratio (S/N) of 2 and higher. Elemental formulas were calculated for each peak in batch mode by an in-house–written software tool. In conjunction with an automated theoretical isotope pattern comparison, the generated formulas were validated by setting sensible chemical constraints (N rule; O/C ratio ≤ 1; H/C ratio $\leq 2n+2$; element counts: C ≤ 100, H ≤ 200, O ≤ 80, N ≤ 3, S ≤ 3) and mass accuracy window (set here at $+/-0.2$ ppm). Final formulas were generated and classified into groups containing CHO, CHNO, CHOS, or CHNOS. Based on these groups of m/z ratios, specific mass spectra could be reconstructed.

For high-resolution measurements performed in the positive ionization mode, a total transient length of 4 s was registered in each scan. A narrow band excitation sweep was transmitted in the ion cyclotron resonance (ICR) cell for the center of mass $m/z = 321$. A total number of 1,200 scans were accumulated. In each scan, ions with the nominal mass $m/z = 321$ were isolated in the quadrupole and subjected to ion accumulation in the second hexapole for a duration of 300 ms. Quadrupole ion isolation was necessary to reduce ion columbic repulsion effects in the ICR cell, which limited the attained mass resolving power. Nevertheless, a resolution of more than 1 million could be achieved for all identified signals. In some cases, a resolution exceeding 1.3 million could be reached so that a resolved doublet with a mass difference between both singlets of 1 milli mass unit was detected. This is approximately equivalent to the mass sum of merely two electrons.

NMR Analyses. All experiments in this study were performed with a Bruker DMX 500 spectrometer at 283 K (CD_3OD) with a 5-mm z-gradient $^1H/^{13}C/^{15}N$ TXI cryogenic probe using 90° excitation pulses [90° (^1H) = 10 μs; 90° (^{13}C) = 10 μs]. 1D ^1H NMR were recorded using the first increment of the presat-NOESY sequence (solvent suppression with presaturation and spin-lock, 1 ms mixing time, 5 s acquisition time, 15 s relaxation delay, up to several hundred scans, 1 Hz exponential line broadening). Absolute value COSY and sensitivity-enhanced phase sensitive TOCSY NMR spectra used spectral widths of 6,009 Hz with acquisition times of 681 ms (relaxation delay: 819 ms for COSY and 2,819 ms for TOCSY) and a dipsi2-mixing time of 70 ms; number of scans were up to 512 and number of increments up to 1,024. Sensitivity-enhanced ^1H, ^{13}C HSQC of methanolic extract used acquisition time: 150 ms at spectral width of 5,482 Hz; ^{13}C-90° decoupling pulse, GARP (70 μs); $^1J(CH) = 150$ Hz, 1.35 s relaxation delay; F1 (^{13}C): SW = 22,014 Hz (175 ppm); number of scans(F2)/F1-increments (^{13}C frequency): (512/406). Gradient (1 ms length, 450 μs recovery) and sensitivity-enhanced sequences were used for HSQC and TOCSY but not COSY spectra. References used were CD_3OD (3.30/49 ppm), CD_3CN (1.93 ppm), CD_2Cl_2 (5.35 ppm). Homonuclear 2D NMR spectra were computed into a $8,192 \times 1,024$ matrix with exponential line broadening of 2.5 Hz in F2 and a shifted sine bell (π/2.5) in F1.

Ultraperformance Liquid Chromatography Coupled to Quadrupole Time of Flight Mass Spectrometry Analysis. The analyses were performed on a Waters Acquity UPLC™ (Waters, Eschborn, Germany) system. The chromatographic analyses were carried out on Vision C18-HL with particle size of 1.5 μm and column dimension of 2.1×150 mm (Alltech-Grom, Rottenburg-Hailfingen, Germany). Linear solvent strength gradient from 5% ACN in water containing 0.1% formic acid to 100% ACN within 60 min was applied. The column was thermostated to 35 °C, and the flow rate of the eluent was 0.25 mL/min, resulting in a maximal pressure of 760 bar. The injection volume was set to 3 μL via partial loop injection.

The ultraperformance liquid chromatography (UPLC) was coupled online with a SYNAPT™ mass spectrometer (Waters, Eschborn, Germany) via electrospray interface operating at positive mode. The disolvatation gas and the cone gas were set to 800 L/h and 50 L/h, respectively. The source temperature was 120 °C, and the capillary voltage of 3 kV and cone voltage of 30 V were applied. The quadruple was operated at broad mass range (from 50 to 2,000 m/z), and the TOF was set to V-shaped optics to increase the instrument sensitivity. The data were collected at centroid mode with acquisition rate of 0.1 s using dynamic range enhancement. Prior to the measurement the MS was calibrated with sodium formiate and the mass precision and repeatability was maintained using lock spray: 400 μg/mL leucine-enkephalin (556.2771 Da) at flow rate of 5 μL/min was infused through a separated spray, and data were collected and recalibrated every 15 s. MassLynx software was used for controlling the instrument and interpreting the acquired data.

Sonification of Experimental Data. Sonification of the raw data (m/z versus intensity) was enabled to complement the statistical data analysis as to enhance the data perception in addition to the data-visualization through the numerous figures in this manuscript.

A very simple transformation was used and can be listened to in the three downloadable files in which the perception of time is given by the mass differences between two consecutive signals and the pitch is rendered by the intensity of the given signals. The schematic representation of that transformation is shown in Fig. S9.

NMR. The structural diversity of the Murchison extracts as reflected by a considerable variance of their NMR spectra refers

to a wide range of aliphatic and aromatic chemical environments. Nevertheless, the signal envelopes of one-dimensional ^{1}H NMR spectra shared common characteristics (Fig S4*A* and *B*). The thousands of compounds identified in FTICR mass spectra display several tens of thousands of individual NMR resonances that appear as strongly superimposed broad envelopes. Still recognizable signals will indicate (groups of) more prominent chemical environments.

Here, the general envelopes in the aliphatic [$\delta(^1\mathrm{H}) = 0.5$ to 2.5 ppm] and aromatic [$\delta(^1\mathrm{H}) = 6$ to 9 ppm] region of the three extracts (CD_2Cl_2, CD_3OD, CD_3CN) all show prominent aliphatic and wide-ranging aromatic NMR resonances. Heteroatom-containing fragments (e.g. HC-X; X = O, N, (S) ; $\delta(^1\mathrm{H}) = 2.5$ to 5.5 ppm) exhibit a more distinct variance and increase in occurrence from CD_2Cl_2 to CD_3OD extracts.

In all extracts, aromatic protons indicate a wide range of direct ortho and/or para-oxygenation ($\delta(^1\mathrm{H}) < 7$ ppm) and carbonyl derivatives ($\delta(^1\mathrm{H}) > 7.3$ ppm) in case of isolated rings; polycyclic aromatic compounds (possibly more concentrated in CD_2Cl_2 extracts) and/or N-heterocycles also resonate within this chemical shift region. Nonpolarized double bonds with $\delta(^1\mathrm{H}) = 5$ to 6 ppm are considered not prominent in Murchison organic extracts.

The nature of the selective extracts designed to improve the quality of the FTICR mass spectra implied considerable dilution of compounds, causing limited S/N ratios in NMR spectra. Therefore, proton-detected spectra were mainly restricted to homonuclear 2D NMR spectra, and shorter transfer time (1/2J instead of 1/J) as well as in-phase magnetization contributed to better S/N ratios of TOCSY cross peaks in comparison with COSY cross peaks, especially in the aromatic section (Fig. S4*C*–*N*).

Methanolic extract COSY NMR spectra revealed a very wide range of aliphatic cross peaks of terminal methyl within short (C_2-C_4) chains, indicating a very substantial variability in aliphatic branching. The cross peaks originating from chain terminations (>50) appear as numerous as intraaliphatic (HC-CH) cross peaks. Aromatic rings and/or carbonyl derivatives induce slight downfield proton shift displacement [$\delta(^1\mathrm{H}) = 2$ to 3 ppm] for associated aliphatic residues. The number of cross peaks relating both of these positions is minor. Oxygen-containing fragments related to ethers and esters (C-HC-CH-O) are more numerous than those of intraoxygen functionalization (O-HC-CH-O). Aromatic substitution patterns, as deduced from TOCSY NMR spectra, especially within CD_2Cl_2 and CD_3CN extracts, appear to contain both oxygen and carbonyl attached to aromatic rings [the downfield NMR resonances ($\delta(^1\mathrm{H}) > 7.5$ ppm) in CD_2Cl_2 extracts could be caused by polycyclic aromatics; Fig. S4*J*–*N*].

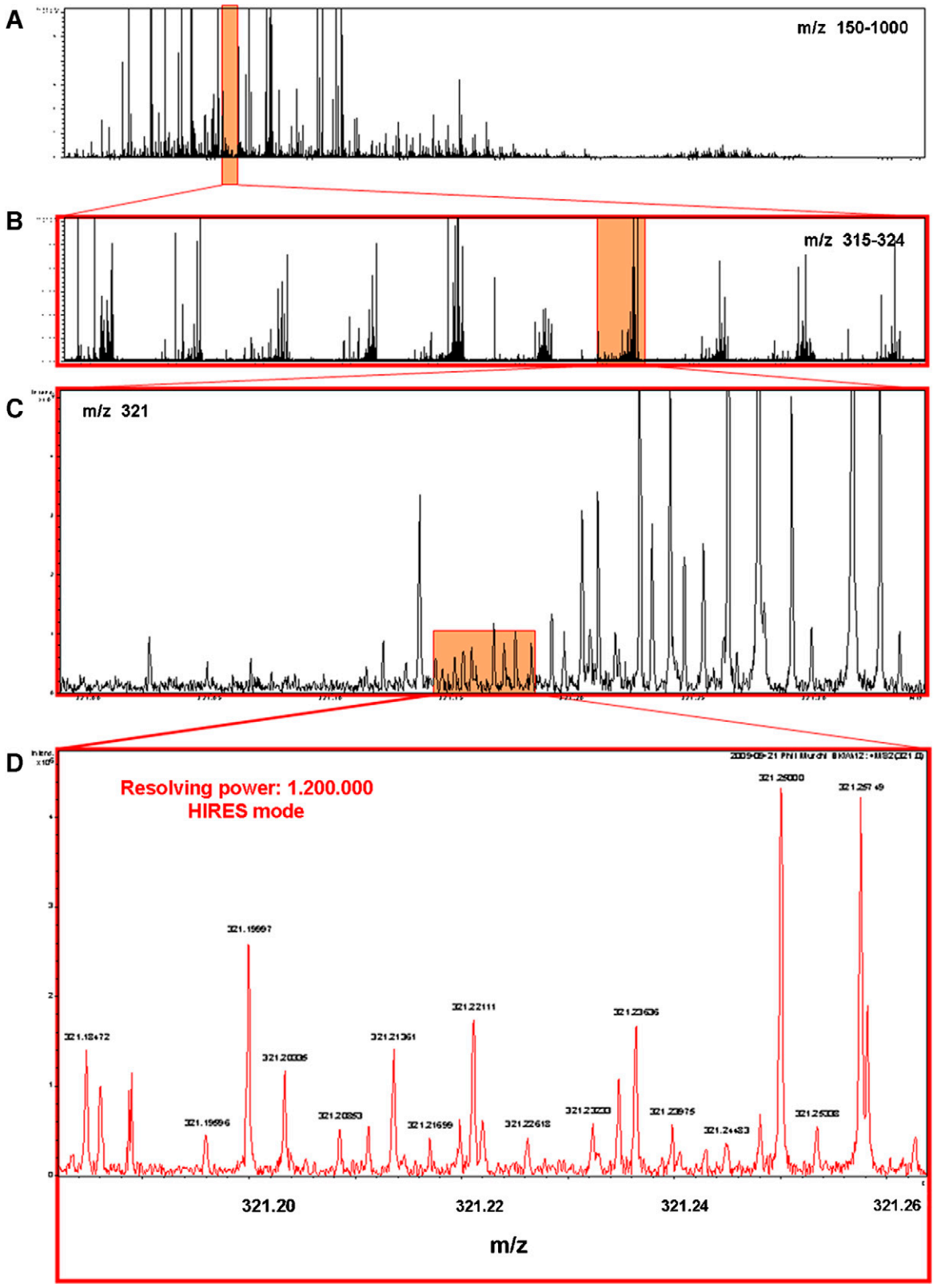
A
m/z 150-1000
B
m/z 315-324
C
m/z 321
D
Resolving power: 1.200.000
HIRES mode
321.15697
321.18472
321.20006
321.15596
321.20853
321.21361
321.21699
321.22111
321.22618
321.23636
321.23220
321.22975
321.24483
321.25000
321.25308
321.25749
321.20
321.22
321.24
321.26
m/z

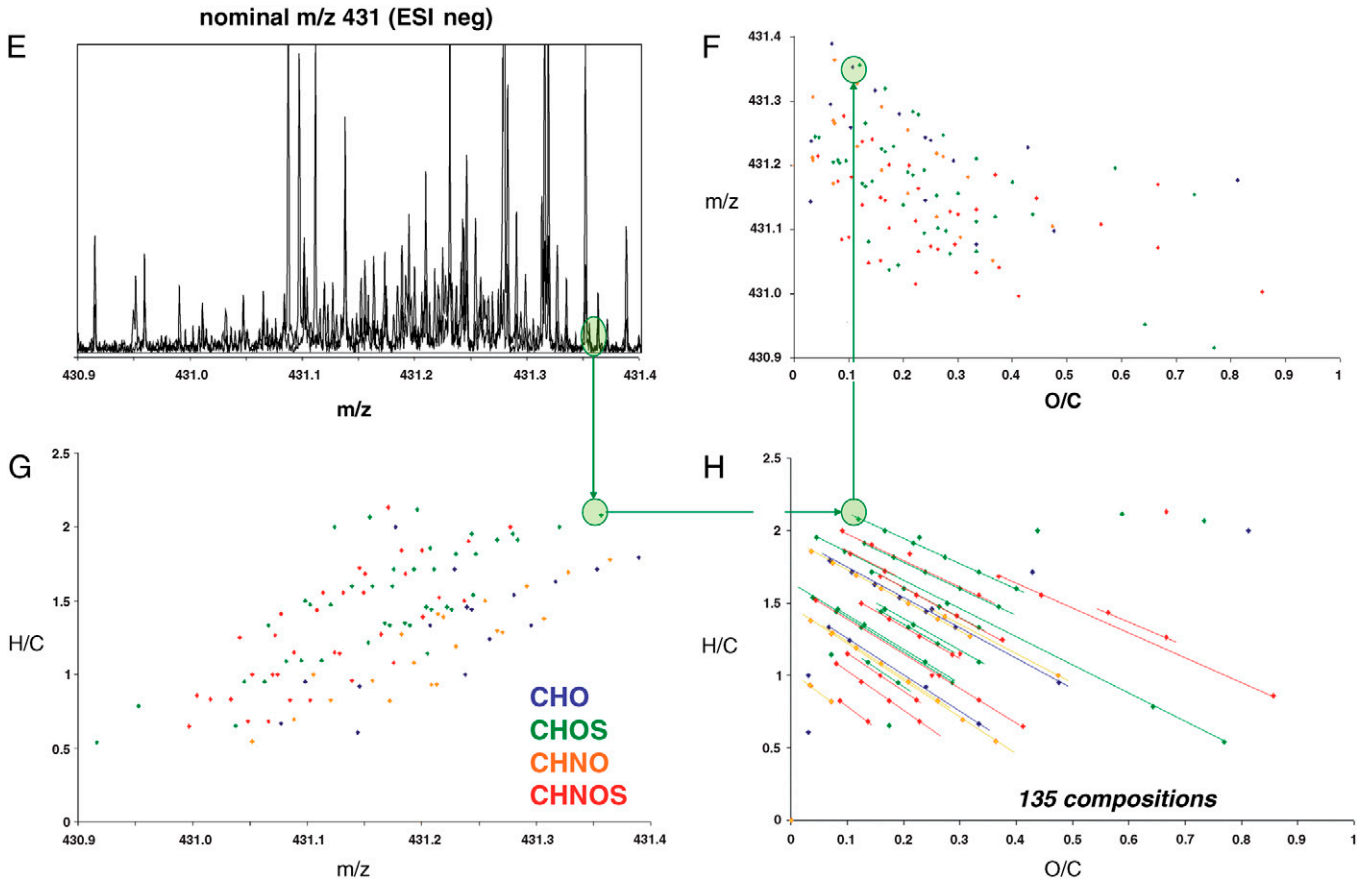

Fig. S1. Progressive detailed visualization of the methanolic Murchison extract in the positive modus ESI FTICR/MS spectra in the mass ranges (*A*) 150–1000 Da, (*B*) 315–324 Da, (*C*) 321.0–321.35 Da, and (*D*) high-resolution (HIRES) mode in 321.180–321.266 Da. Integrated representations of the molecular diversity in the methanol extracted fraction, derived from ESI(−) FTICR/MS spectra (*E*) at nominal mass 431 Da. (*F–H*) Relationships between *m*/*z*, H/C, and O/C elemental ratios corresponding to the mass spectra shown in *E*. Note that 26 different CH_4/O series related by a formal exchange of CH_4 against oxygen could be observed in the van Krevelen diagram corresponding to the nominal mass 431 Da (*H*).

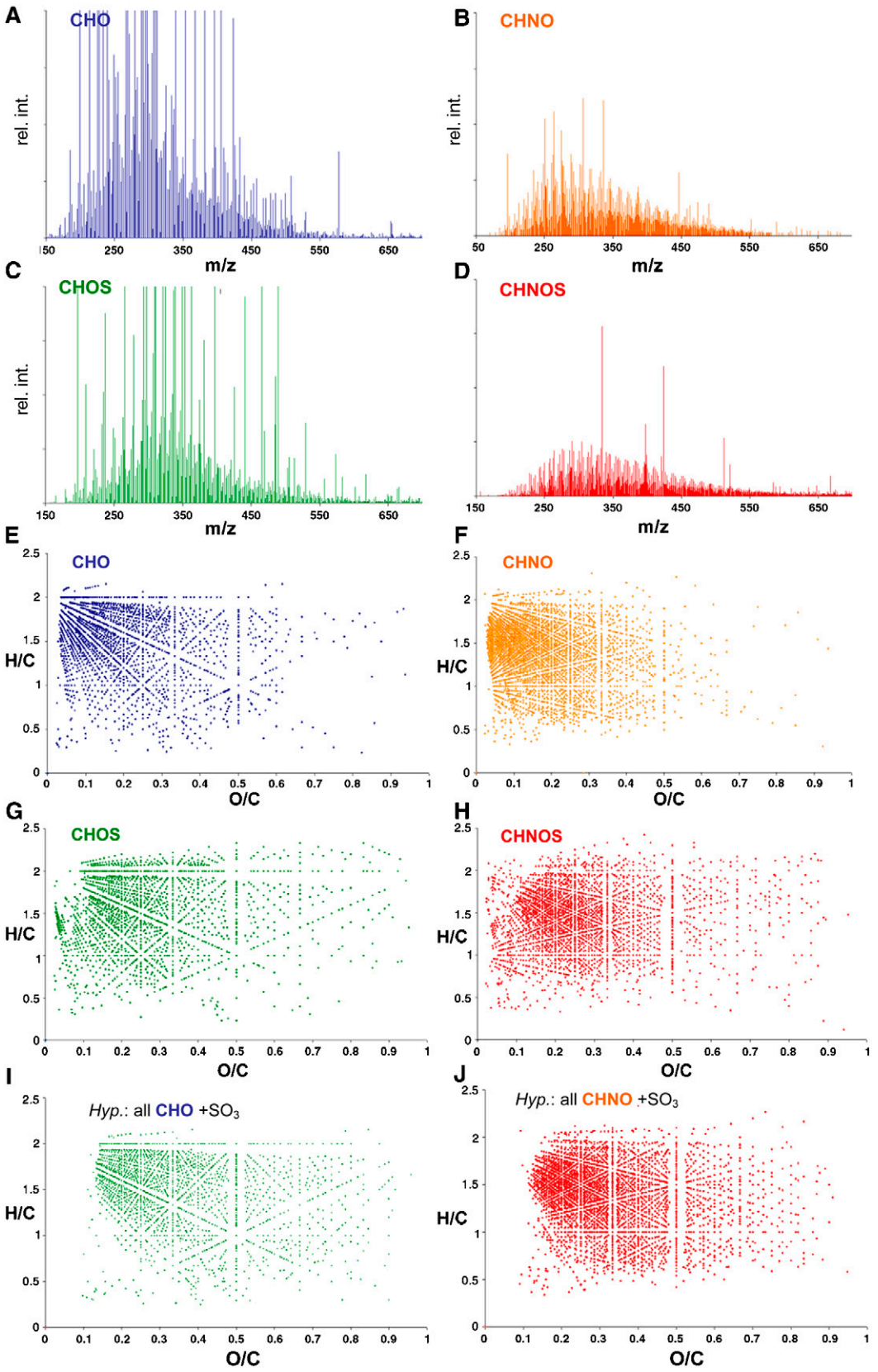

Fig. S2. (*A–D*) Reconstructed mass spectra showing the mass distributions and (*E–H*) van Krevelen diagrams specific for CHO, CHOS, CHNO, and CHNOS elemental compositions of Murchison methanolic extract from ESI(–) FTICR mass spectra. The most intense signals protruding from the regular distribution patterns correspond to impurities such as contaminations and/or degradation end-products. (*I* and *J*) van Krevelen diagrams obtained under the hypothesis of SO_3 added to (*I*, *E*) CHO and (*J*, *F*) CHNO series (conversion of C-OH into C-OSO_3H).

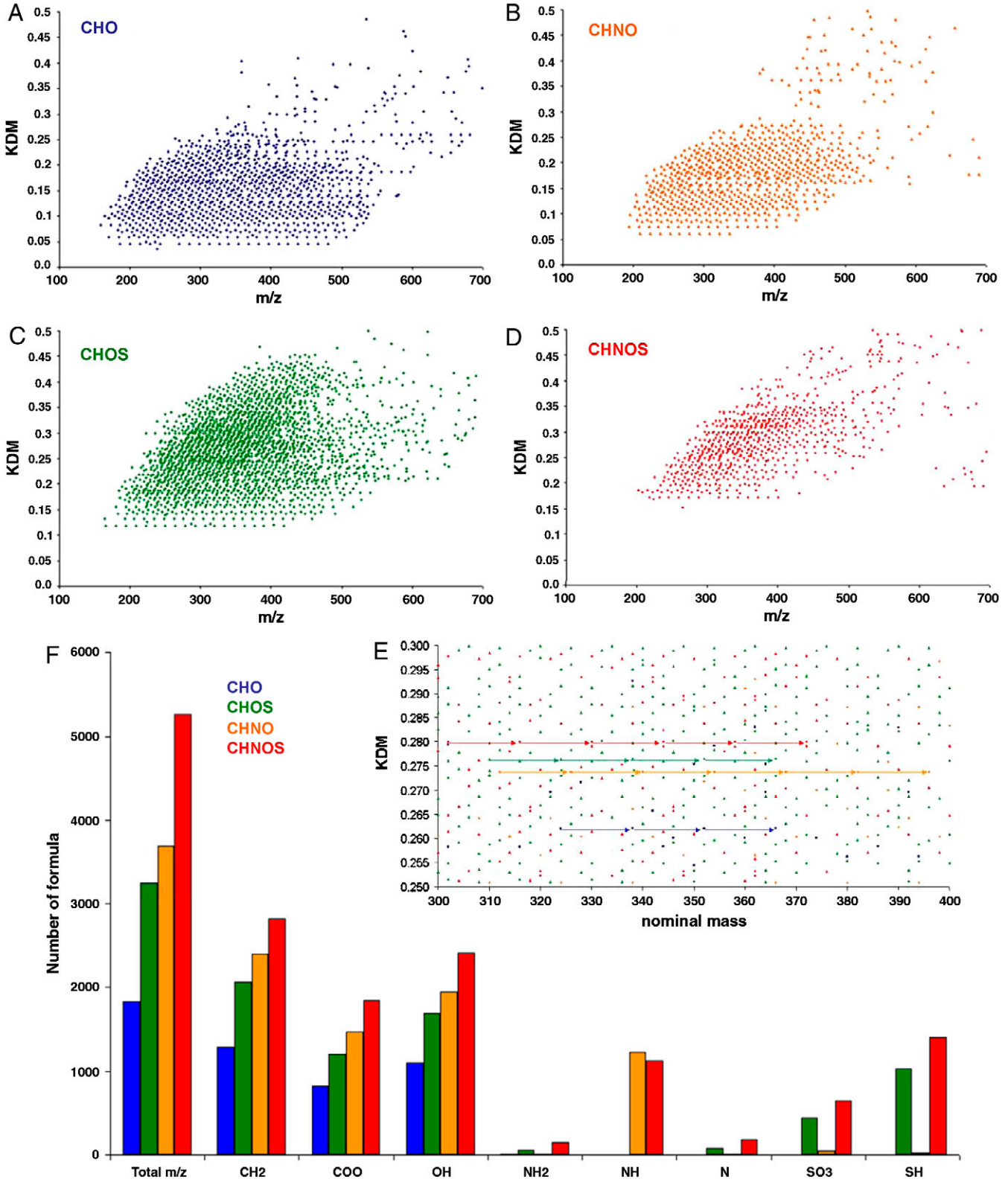

Fig. S3. (*A–D*) CH_2-Kendrick mass diagrams specific for CHO, CHOS, CHNO, and CHNOS elemental compositions. (*E*) Detail in CH_2-Kendrick mass diagrams specific for CHO, CHOS, CHNO, and CHNOS elemental compositions. (*F*) Number of *m/z* signals involved in pairs having an exact *m/z* difference (at 0.5 ppm) corresponding to a change in functionality: methylene, carboxylic, hydroxyl, amine (primary, secondary, tertiary), SO_3, or SH.

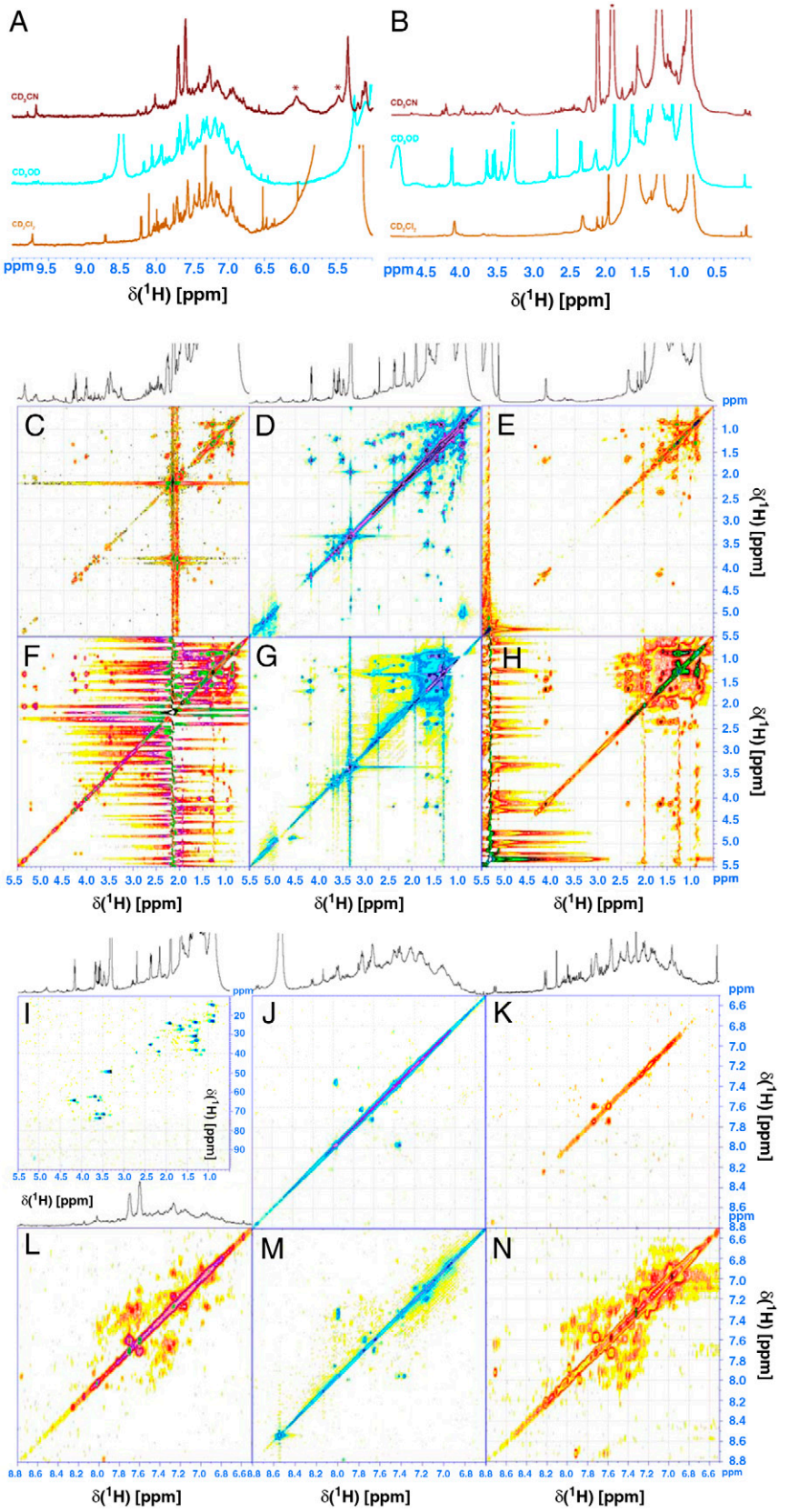

Fig. S4. (*A–B*) ^{1}H NMR spectra (500 MHz) of Murchison organic extracts of (*A*) low field [$\delta(^{1}H)$: 10–5 ppm] and (*B*) high field [$\delta(^{1}H)$: 5–0 ppm] sections; from top to bottom: CD_3CN (* denotes solvent signals), CD_3OD, CD_2Cl_2. (*C–H*) COSY and TOCSY NMR spectra of Murchison extract, aliphatic section. Top row (*C–E*): COSY NMR spectra of CD_3CN, CD_3OD, CD_2Cl_2 (from left to right) and bottom row (*F–H*) TOCSY NMR spectra of CD_3CN, CD_3OD, CD_2Cl_2 (from left to right). (*J–N*) COSY and TOCSY NMR spectra of Murchison extract, aromatic section. Top row (*I*): ^{1}H, ^{13}C HSQC and (*J*) COSY NMR spectra of methanolic extract, (*K*) COSY NMR spectrum of CD_2Cl_2 extract. Bottom row (*L–N*) TOCSY NMR spectra of CD_3CN, CD_3OD, CD_2Cl_2 extracts (from left to right).

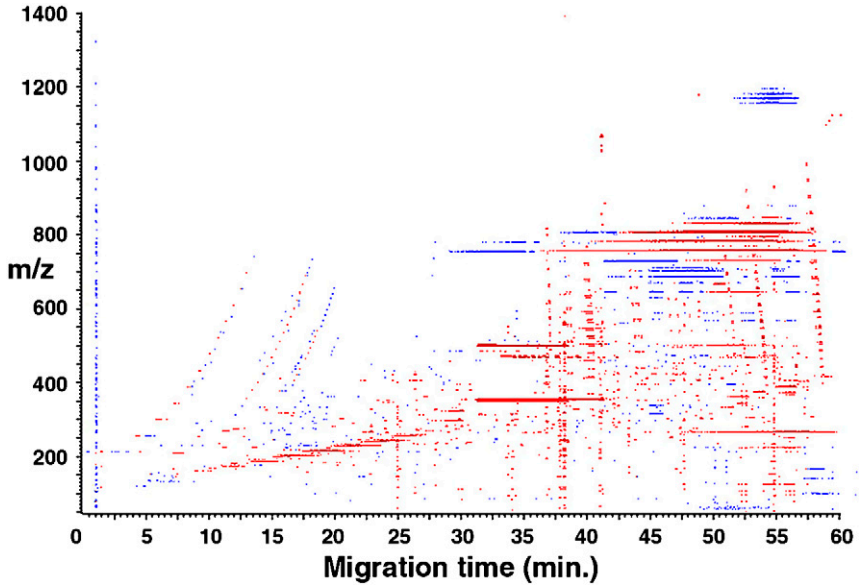

Fig. S5. UPLC–ESI(–)QTOF/MS diagrams of Murchison methanol (blue) and acetonitrile (red) extracts showing extended molecular series with characteristic mass differences of 14 or 44 Da. A larger retention times, higher masses within molecular series exhibit comparatively lesser retention time because of enhanced interaction with the separation column, likely induced by increased relative aliphaticity.

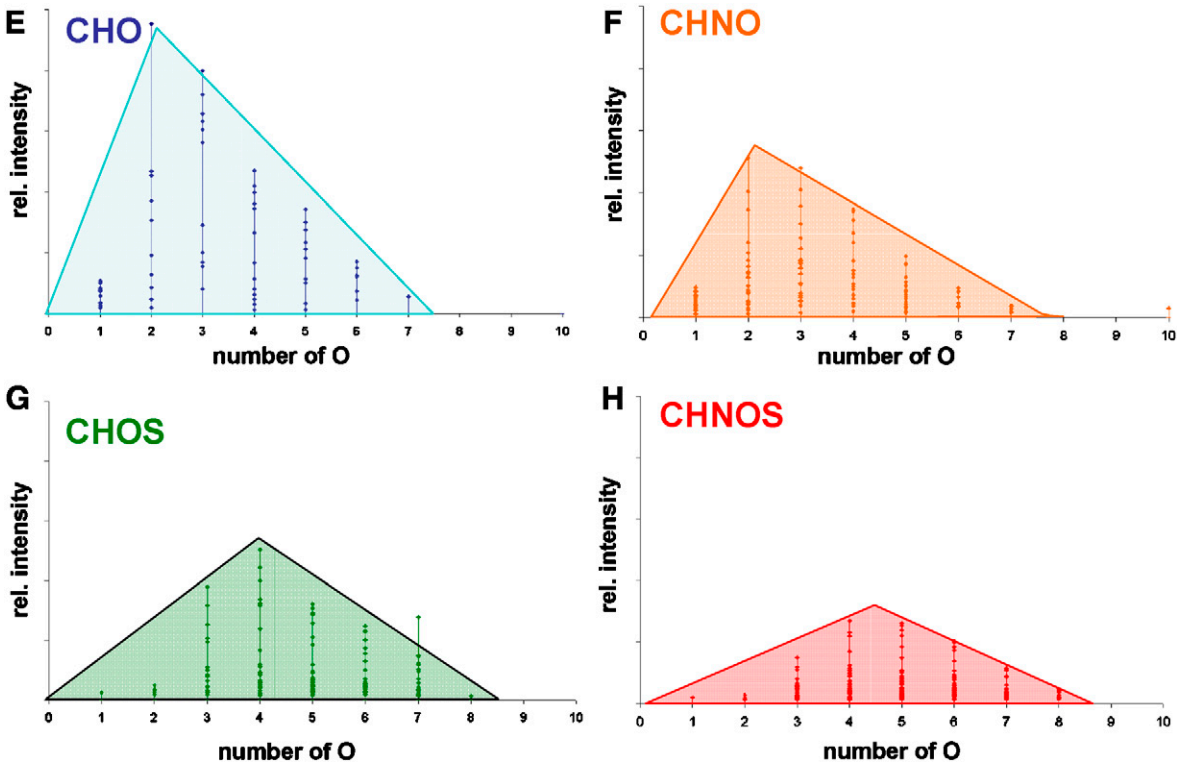

Fig. S6. (*A–D*) Mass peak distribution of molecular series with different elementary compositions when considering the number of hydrogen atoms (vertical axis) versus carbon atoms (horizontal axis). Circle areas are related to the mass peak intensities, and singular large peaks out of the regular signal distributions likely denote terrestrial contamination. Note that CHO and CHOS are closely similar in their distributions, as well as CHNO and CHNOS molecular series. (*E–H*) Mass peak distribution of molecular series with different elemental compositions when considering the number of oxygens (horizontal axis) and their intensity (vertical axis) only for the components bearing 19 carbons. Here the CHO, CHNO, CHOS, and CHNOS are closely similar in their distributions showing the increase in oxygen atoms along with the integration of sulfur.

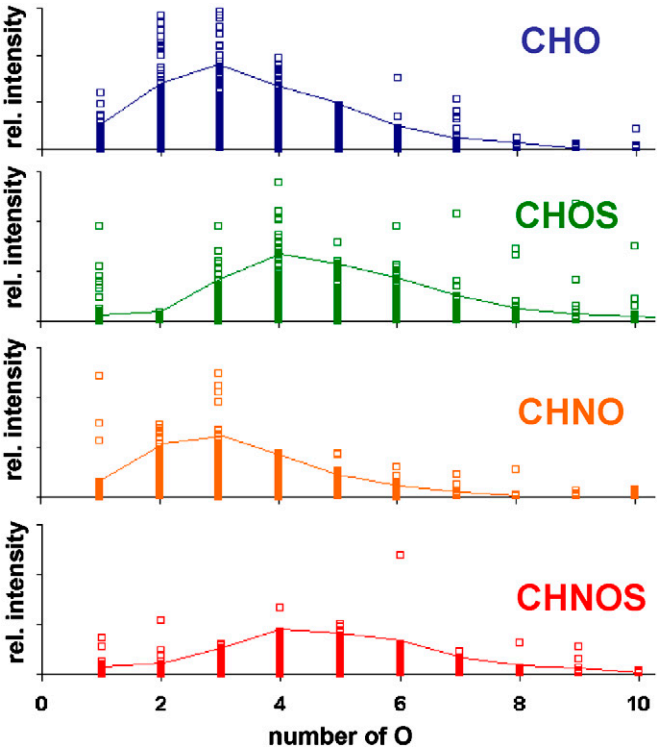

Fig. S7. Mass peak distribution within the different molecular series of elemental compositions when considering the number of oxygen atoms (horizontal axis) and their intensity (vertical axis) for all signals. The horizontal displacement of CHOS against CHO and CHNOS against CHNO series indicates occurrence of sulfur in elevated oxidation states.

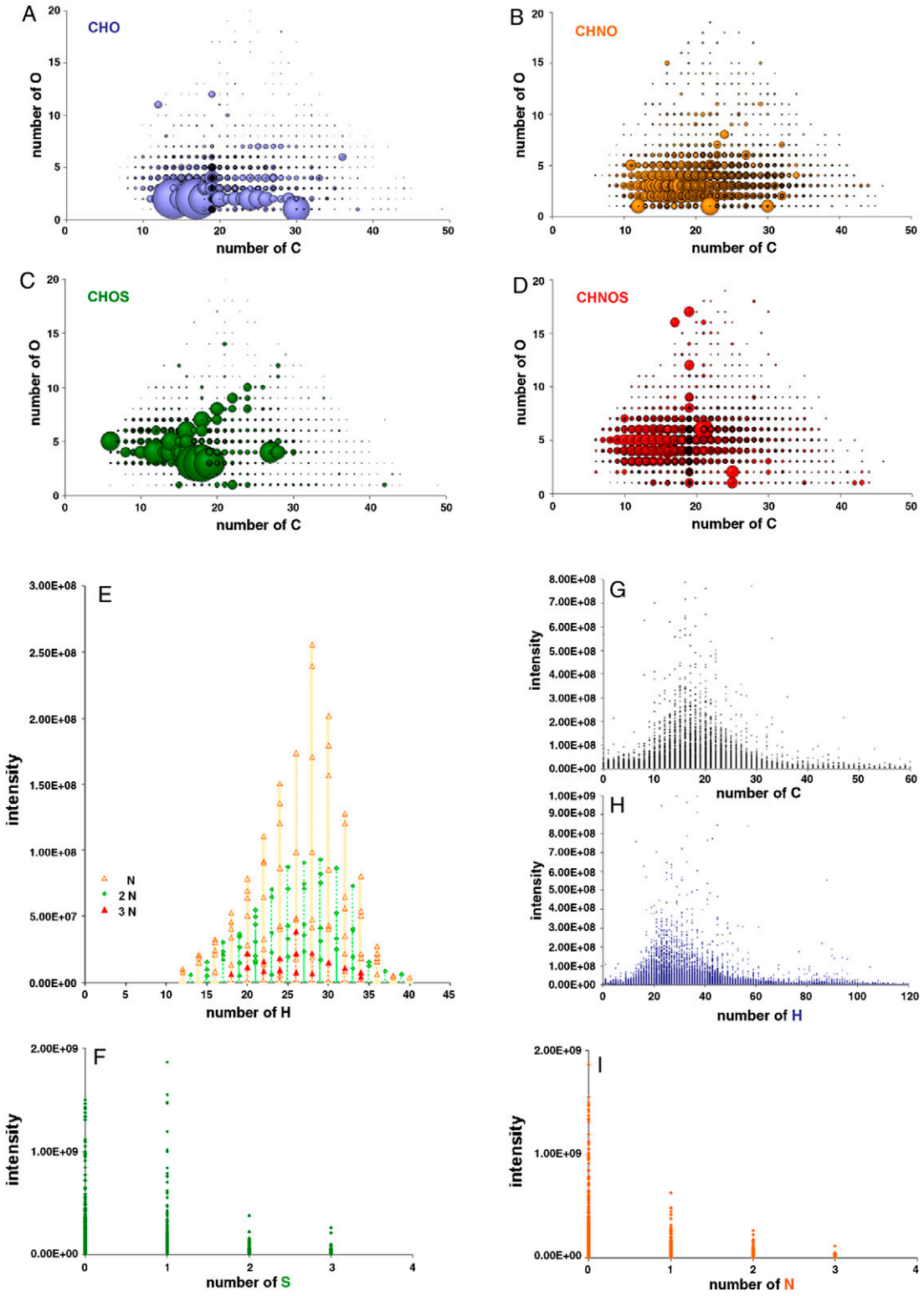

Fig. S8. (*A–D*) Distribution of mass peaks within the molecular series of different elemental compositions when considering the number of oxygen atoms (vertical axis) versus carbon atoms (horizontal axis). Circle areas are related to mass peak intensities; here, singular large peaks likely denote terrestrial contamination. (*E–I*) Atom frequency derived from ESI(–) FTICR mass spectra of Murchison methanol extracts (*E*) within all CHN compositions involving only 19 carbons. The skew from a Gaussian distribution toward lesser numbers of hydrogen likely denotes the increased options of nitrogen-heterocyclic compounds to form chemically reasonable isomers as opposed to otherwise structure analogous carbocycles; decrease of peak intensity for all masses with the increase of (*F*) the number of S atoms and (*I*) the number of N atoms; (*G* and *H*) near Gaussian signal distribution of the number of C and H atoms.

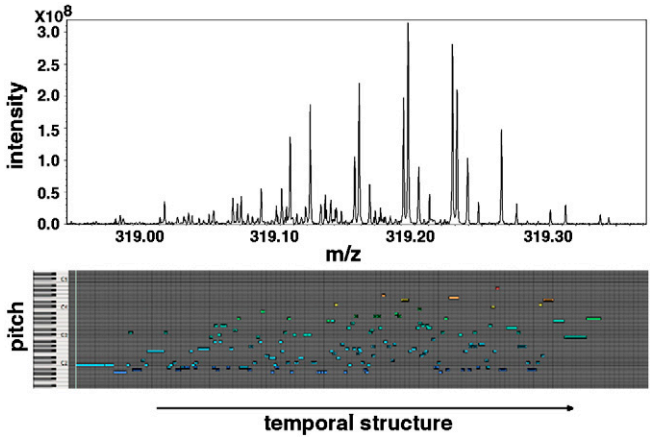

Fig. S9. Scheme used for the sonification of the data showing the nominal mass 319 out of Fig. 1*C* and the corresponding transformations for the notation (the signal intensity giving the pitch of the sound and the $\Delta m/z$ giving the temporal structure).

Other Supporting Information Files

Supporting Online Audio files S10: Listen to sonified ultrahigh-resolution mass spectrometric data; *S10a*: m/z 319, methanol extract analyzed in ESI(−) mode as illustrated in Fig. 1*C*, and hear in *S10b* the similarity to the signal distributions in nominal mass m/z 431 as illustrated in Fig. 3; *S10c*. Nominal mass m/z 431 was also sonified from the ethanol extract ESI(−) FTICR/MS raw data.

Audio File S10a (MP3)
Audio File S10b (MP3)
Audio File S10c (MP3)